Magnetic and Quasiparticle Spectra of an itinerant $J_1 - J_2$ Model for Iron Pnictides

C. M. S. da Conceição,[1] M. B. Silva Neto,[2] and E. C. Marino[2]

[1] *Departamento de Física Teórica, Universidade do Estado do Rio de Janeiro, Rio de Janeiro, RJ 20550-013, Brasil*
[2] *Instituto de Física, Universidade Federal do Rio de Janeiro, Caixa Postal 68528, Brasil*

We calculate the magnetic and quasiparticle excitation spectra of an itinerant $J_1 - J_2$ model for iron pnictides. In addition to an acoustic spin-wave branch, the magnetic spectrum has a second, optical branch, resulting from the coupled four-sublattice magnetic structure. The spin-wave velocity has also a planar directional anisotropy, due to the collinear/striped antiferromagnetism. Within the magnetically ordered phase, the quasiparticle spectrum is composed of two Dirac cones, resulting from the folding of the magnetic Brillouin zone. We discuss the relevance of our findings to the understanding of both neutron scattering and photoemission spectroscopy results for $SrFe_2As_2$.

PACS numbers: 78.30.-j, 74.72.Dn, 63.20.Ry, 63.20.dk

arXiv:1004.3187v2 [cond-mat.str-el] 12 Apr 2011

Since the discovery of superconductivity above 50 K in $RFeAsO_{1-x}F_x$ (R = La, Ce, Sm, etc.) [1], the term *high temperature superconductivity* can no longer be associated exclusively to cuprates. The new iron-based pnictide compounds, including the MFe_2As_2 (M = Ba, Sr, etc.) family [2], exhibit, just like cuprates, a layered antiferromagnetic (AF) structure in the parent compound, which gives room to superconductivity upon doping [3]. One important difference, however, is related to the transport and optical properties of their parent compounds. While cuprates are Mott antiferromagnetic insulators, pnictides are metals, albeit not very good ones, with a very rich multi-band Fermi surface [4]. Despite this difference, it is believed that, in both cases, strong correlations of strength U among transition metal electrons, from Cu in the case of cuprates and from Fe in the case of pnictides, play a very important role [5]. In fact, it has been argued that, at zero temperature, $T = 0$, these two systems could be represented as very closely, but at oposite sides, to a Mott metal insulator transition, in the $T \times U$ phase diagram [5]. This would explain, for example, the experimentally observed strong renormalization of the coherent quasiparticle spectral weight at the Fermi level in pnictides [6], which would be shifted to form incoherent lower and upper Hubbard bands, just like in prototypical Mott insulators such as cuprates.

The incoherent part of the spectrum in iron pnictides can be well described in terms of localized moments at the Fe positions, interacting via a superexchange J_1 between nearest Fe neighbors, Fe−Fe, and a second superexchange J_2 between As bridged next-to-nearest Fe neighbors, Fe−As−Fe [7]. Alternatively, an itinerant description, in terms of coherent multi-band electrons and holes, Fermi surface nesting, and spin-density-wave (SDW) instability, can also be used for the understanding of both the antiferromagnetic and superconducting states in iron pnictides [8, 9]. In this letter, we shall adopt a combined description, merging these two degrees of freedom, in which local magnetic moments are coupled, via Hund's exchange interaction [10], to itinerant quasiparticles, to be described by a minimal two-band model [11].

Let us start by analyzing the magnetic excitation spectrum. One important difference between having $S = 1/2$, as in cuprates, or $S = 1$ (or higher), as in pnictides, is the possibility of single ion anisotropy, in the later case, which arises from relativistic corrections and the spin orbit coupling. The simplest model that captures all the essential local moment physics described in the previous paragraphs is the extended $J_1 - J_2$ spin-Hamiltonian

$$\hat{H} = J_1 \sum_{\langle i,j \rangle} \hat{\mathbf{S}}_i \cdot \hat{\mathbf{S}}_j + J_2 \sum_{\langle\langle i,j \rangle\rangle} \hat{\mathbf{S}}_i \cdot \hat{\mathbf{S}}_j - K \sum_i (\hat{S}_i^z)^2, \quad (1)$$

where $J_1 > 0$ and $J_2 > 0$ are, respectively, the antiferromagnetic superexchanges between nearest-neighbors, $\langle i,j \rangle$, and next-to-nearest neighbors, $\langle\langle i,j \rangle\rangle$, spins $\hat{\mathbf{S}}_i$ on a two dimensional square lattice, and $K > 0$ is the single ion anisotropy coupling constant.

The existence of two superexchanges J_1 and J_2 in the spin Hamiltonian (1) renders the antiferromagnetism collinear, with wave vectors at $(\pi, 0)$ and/or $(0, \pi)$ [13]. This is in agreement with inelastic neutron scattering in $(Sr,Ba)Fe_2As_2$ [13, 14], which exhibit peaks at the AF zone center $Q = (1, 0, 1)$, for energies between $5-15$ meV. This situation is markedly different from a Néel ordered state with wave vector at (π, π), as found in cuprates, where a single superexchange J between Cu−O−Cu is present. As discussed in the literature, such wave vector degeneracy in the classical ground state of the Hamiltonian (1) gives rise to an extra Ising symmetry [15–17], which is broken at a different temperature than the AF ordering one. The hierarchy of symmetry breaking as T is lowered is: paramagnetic (PM)/Ising symmetric, PM/Ising broken, and AF/Ising broken phases [16].

Previous linear spin wave studies of the $J_1 - J_2$ model with $K = 0$ have considered, as a starting point, a classical ground state with a *two sublattice structure*, and have obtained that the quantized magnetic spectrum would be composed by a single gapless spin-wave branch [18], with $\hbar\omega(\mathbf{k}) \sim |\mathbf{k}|$ for small wave vector $\mathbf{k}$. The existence of such gapless mode reflects the full rotational invariance of the spin Hamiltonian (1), when $K = 0$, and is in agreement with Goldstone's theorem. We shall refer to this

branch as the *acoustic branch*. On the other hand, inelastic neutron scattering revealed the gapped nature of the magnetic spectrum [13, 14], indicating that the single-ion anisotropy parameter $K \neq 0$. However, the absence of a clean step in the neutron integrated intensity (expected for the case of a single gap), makes room for the existence of two or more magnetic branches [13, 14]. As we shall soon see, the actual *four sublattice structure* of the AF/Ising broken classical ground state, with two coupled, interpenetrating Néel ordered states, gives rise to a second, optical spin-wave branch (already for $K = 0$). Below we will consider $K \neq 0$, when rotational invariance is broken and all branches become gapped.

In order to understand the origin of the optical mode in the $J_1 - J_2$ Hamiltonian (1) it suffices to consider the isotropic case, $K = 0$. For $J_2 \simeq 2J_1$, as the experiments suggest, the ground state is a collinear antiferromagnet, composed by two coupled, interpenetrating Néel ordered states We span spins in a coherent basis for each of these Néel states, which we label as A and B, and we write $\hat{\mathbf{S}}_i^A = S\mathbf{\Omega}_i^A = S\left[e^{\mathrm{i}\mathbf{Q}\cdot\mathbf{x}_i}\mathbf{n}_A(\mathbf{x}_i)\sqrt{1-\left(\frac{\mathbf{L}_A}{\bar{s}}\right)^2}+\frac{\mathbf{L}_A}{\bar{s}}\right]$, and $\hat{\mathbf{S}}_i^B = S\mathbf{\Omega}_i^B = S\left[e^{\mathrm{i}\mathbf{Q}\cdot\mathbf{x}_i}\mathbf{n}_B(\mathbf{x}_i)\sqrt{1-\left(\frac{\mathbf{L}_B}{\bar{s}}\right)^2}+\frac{\mathbf{L}_B}{\bar{s}}\right]$, where $\mathbf{Q} = (\pi/a, \pi/a)$ is the ordering wave vector for each Néel state, $\mathbf{n}_{A,B}$ and $\mathbf{L}_{A,B}$ are, respectively, the staggered and uniform components of the spins belonging to the two states, and $\bar{s} = S/a^d$ is the density of spin in the unit cell. We use the constraint $\mathbf{n}_{A,B}^2 = 1$.

After integrating out the uniform (fast) components $\mathbf{L}_A$ and $\mathbf{L}_B$ of the spins we arrive at the action of the nonlinear sigma model for the case $K = 0$ (the detailed derivation of this model will appear elsewhere [12]). This action describes the low-energy, long-wavelength fluctuations of the staggered (slow) order parameter $\mathbf{n}_{A,B}$ (as usual we use $\beta = 1/k_BT$ and $\int = \int_0^{\hbar\beta} \mathrm{d}\tau \int \mathrm{d}^2\mathbf{x}$)

$$\begin{aligned}\mathcal{S} &= \frac{\rho_s}{2\hbar}\int\Big\{\left(|\nabla\mathbf{n}_A|^2+|\nabla\mathbf{n}_B|^2\right)+\frac{1}{c_0^2}\left(|\partial_\tau\mathbf{n}_A|^2+|\partial_\tau\mathbf{n}_B|^2\right)\\ &+ \gamma\left(\mathbf{n}_A\cdot\partial_x\partial_y\mathbf{n}_B+\mathbf{n}_B\cdot\partial_x\partial_y\mathbf{n}_A\right)+\eta\,\mathbf{n}_A\cdot\mathbf{n}_B\\ &+ \mathrm{i}b\left[\mathbf{n}_A\cdot(\mathbf{n}_B\times\partial_\tau\mathbf{n}_B)+\mathbf{n}_B\cdot(\mathbf{n}_A\times\partial_\tau\mathbf{n}_A)\right]\\ &- \frac{1}{c_1^2}\left[(\mathbf{n}_A\cdot\mathbf{n}_B)(\partial_\tau\mathbf{n}_A\cdot\partial_\tau\mathbf{n}_B)-(\mathbf{n}_A\cdot\partial_\tau\mathbf{n}_B)(\mathbf{n}_B\cdot\partial_\tau\mathbf{n}_A)\right]\Big\}\end{aligned} \quad (2)$$

The first line describes the low-energy, long-wavelength fluctuations of the two order parameters $\mathbf{n}_A, \mathbf{n}_B$, independently. The second line contains their coupling, through γ, within the AF/Ising broken phase, where the term $\mathbf{n}_A \cdot \mathbf{n}_B$ is allowed (this model was derived for the $(\pi, 0)$ magnetic configuration, which breaks explicitly the Ising symmetry). For the Ising symmetric part of the phase diagram, such term would have been absent, but integration over fluctuations would give rise, instead, to a term like $(\mathbf{n}_A \cdot \mathbf{n}_B)^2$, which is Ising invariant [15]. The third line contains a dynamical term that describes the Bloch precession of the staggered moments in a given Néel state (say A) around the moments of the other (say B), and it resembles the coupling to a magnetic field. Finally, the fourth line contains interacting dynamical terms that also arise from the integration over $\mathbf{L}_{A,B}$.

All couplings in (2) are expressed in terms of the original parameters. The spin stiffness is $\rho_s = 2J_2S^2a^{2-d}$, the spin-wave velocity equals $c_0 = 2\sqrt{2}Sa\sqrt{4J_2^2 - J_1^2}/\hbar$, we will also have a contribution from $c_1 = c_0(J_2/J_1)$, while the couplings between $\mathbf{n}_A$ and $\mathbf{n}_B$ are given by $\gamma = \frac{2J_1}{J_2}\left(1+\frac{J_1^2/4}{4J_2^2-J_1^2}\right)$, $\eta = \frac{2}{a^2}\left(\frac{J_1}{J_2}\right)\frac{J_1^2}{4J_2^2-J_1^2}$, and finally $b = \frac{2\hbar J_1}{S^2}\frac{1}{(4J_2^2-J_1^2)}$. The bare (unrenormalized) values of the parameters described above are, as expected, higher than the measured values. For example, for $a = 5.695$ Å, $J_1 = 20$ meV,and $J_2 = 40$ meV, we find $\hbar c_0 = 1.2$ eV Å, while the typical values are actually around 0.25 eV Å. The theory described by Eq. (2) is highly interacting and a full renormalization procedure is required to reproduce the actual values of all couplings and the smallness of the Fe magnetic moment [12]. For the purposes of comparison with experiments in this letter, we shall use the already established values for some of these constants.

To find the magnetic excitation spectrum we look at the poles of the staggered spectral function, $\mathcal{A}(\mathbf{k}, \omega)$. Within the Green's function formalism, these are obtained from the imaginary part of the retarded Green's function, $G_{ret}(\mathbf{k}, \omega)$, for transverse staggered fluctuations $\mathcal{A}(\mathbf{k}, \omega) = -(1/\pi)\lim_{\delta\to 0}\mathcal{I}m[G_{ret}(\mathbf{k}, \mathrm{i}\omega_n \to \omega + \mathrm{i}\delta)]$, where $\omega_n = 2\pi n/\beta$ are the Matsubara frequencies. The first set of poles corresponds to

$$\hbar\omega(\mathbf{k}) = \hbar\, c_{SW}\sqrt{\mathbf{k}^2 + \gamma k_x k_y}, \quad (3)$$

where $\frac{1}{c_{SW}^2} = \left(\frac{1}{c_0^2} - \frac{\sigma^2}{2c_1^2}\right)$. This is the usual acoustic spin-wave branch also found in linear spin wave theory [18], which is gapless at the zone center, $\hbar\omega(0) = 0$, in agreement with Goldstone's theorem. Notice that the observable spin-wave velocity c_{SW} *increases* by a factor $\sqrt{2+\gamma}$ as one moves from the $k_y = 0$ (or $k_x = 0$) line to the $k_x = k_y$ direction (along the spin stripes), showing that the spin-wave dispersion has a *planar directional anisotropy*, see Fig. 1, a consequence of the collinear character of the antiferromagnetic order. The second set of poles corresponds to

$$\hbar\Omega(\mathbf{k}) = \hbar\, c_{op}\sqrt{\mathbf{k}^2 - \gamma k_x k_y + \eta}, \quad (4)$$

where $\frac{1}{c_{op}^2} = \left(\frac{1}{c_0^2} + \frac{\sigma^2}{2c_1^2}\right)$. Here, instead, we find an optical gap, $\hbar\Omega(0) = \Delta_{op} \neq 0$, at the antiferromagnetic zone center $(1, 0, 1)$, given by

$$\Delta_{op} = \hbar\, c_{op}\sqrt{\eta}, \quad (5)$$

which corresponds to long lived optical excitations. Notice now that the optical spin-wave velocity along the $k_x = k_y$ line *decreases* with respect to the $k_y = 0$ (or $k_x = 0$) directions, see Fig. 1, exactly the opposite from

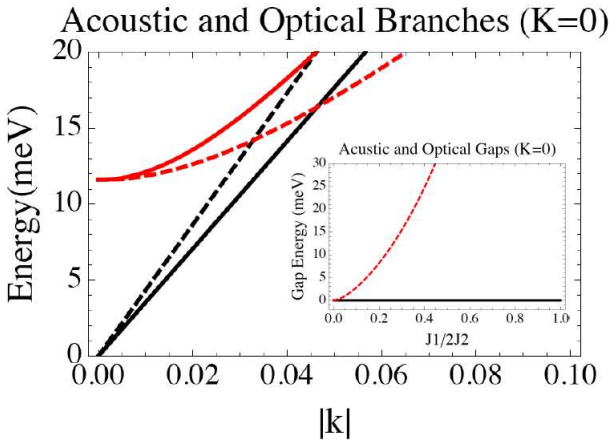

FIG. 1: (Color online): Acoustic (lower, black) and Optical (upper, red) spin-wave branches for the isotropic case, $K = 0$, as a function of $|k|$, for two different directions, $k_y = 0$ (solid lines) and $k_x = k_y$ (dashed lines). Inset: Acoustic and Optical gaps as a function of $J_1/2J_2$. Notice that while the acoustic gap is always zero, as imposed by Goldstone's theorem, the optical gap hardens as J_1 increases, diverging for $J_1 = 2J_2$.

the case for the acoustic branch. The optical gap hardens as J_1 increases, see inset in Fig. 1, and eventually diverges at $J_1 = 2J_2$, when the classical configuration changes and the action (2) has to be modified.

After including a single ion anisotropy (SIA) term at the Fe ions, $K \neq 0$, we have extended the derivation of the nonlinear sigma model accordingly (details will be given elsewhere [12]) and we have recalculated the magnetic excitation spectrum for $K \neq 0$ [12]. The rather lengthy expressions for the dispersions of the two branches for arbitrary K reduce, in the limit $K \ll J_2$, to

$$\hbar\omega(\mathbf{k}) = \hbar\, c_{SW}\sqrt{\mathbf{k}^2 + \gamma k_x k_y + \Delta_{SIA}^2}, \qquad (6)$$

$$\hbar\Omega(\mathbf{k}) = \hbar\, c_{op}\sqrt{\mathbf{k}^2 - \gamma k_x k_y + \Delta_{SIA}^2 + \eta}. \qquad (7)$$

As expected, the immediate effect of a SIA term is to produce a gap for all branches in the spectrum

$$\Delta_{SIA}^2 = \frac{(S-1/2)}{Sa^2}\left(\frac{K}{J_2}\right)\left[1 + \frac{1}{8}\frac{J_1^2}{(4J_2^2 - J_1^2)}\right], \qquad (8)$$

which only exists for high spin systems, being absent when $S = 1/2$, like in the case of cuprates.

We can now analyze recent inelastic neutron scattering results for spin excitations in $SrFe_2As_2$ [13]. The spin-wave dispersion shown in Fig. 2, for scans along $(H, 0, 1)$ at $T = 160$ K, can be well described by the lower branch of the spectrum, $\hbar\omega(\mathbf{k})$, along the $k_x = k_y$ line (we use a coordinate system rotated by 45° with respect to the original unit cell). This branch is gapped solely by the SIA and for $T = 7$ K the gap can be seen at 6.5 meV, see the inset *a*) of Fig. 2. However, as discussed in the introduction, the broadened integrated intensity of the

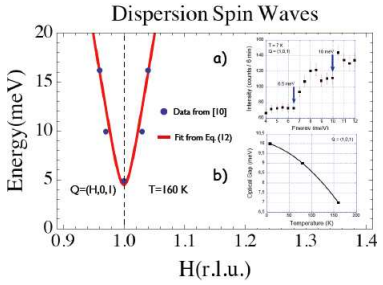

FIG. 2: (Color online): Spin-wave dispersion for $Q = (H, 0, 1)$ and at $T = 160$ K. Experimental data from Ref. [13]. Inset a): integrated intensity at $T = 7$ K, as a function of energy, exhibiting a two-step profile consistent with the existence of two gapped branches in the magnetic spectrum, Eqs. (6) and (7). Inset b): Temperature dependence of the optical gap, according to analysis of the data reported in Ref. [13].

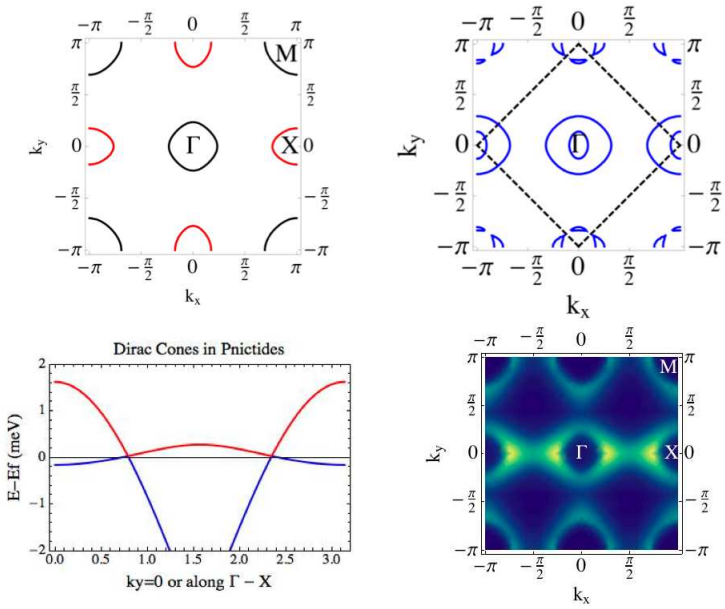

FIG. 3: (Color online): a) (top left) Unfolded two-band Fermi surface; b) (top right) Folded four-band Fermi surface, resulting from the staggered buckling of As ions; c) (bottom left) Dirac cones along the $\Gamma - X$ direction, after folding of the Brillouin zone due to collinear AF order; d) (bottom right) Small hole pockets originating from the top of a Dirac cone.

unpolarized neutrons, observed for either $SrFe_2As_2$ [13] and $BaFe_2As_2$ [14], makes room for the existence of two or more gaps in the magnetic spectrum. In fact, the integrated intensity shown in the inset *a*) of Fig. 2 shows a two-step profile, indicating the presence a second magnon gap at 10 meV. The temperature dependence of the optical gap, following a similar analysis of the data in [13] for $T = 7, 80, 160$ K, is shown in the inset *b*) of Fig. 2.

Next we analyze the quasiparticle excitation spectrum. The introduction of itinerant carriers into the problem presents us with an important question: *if and how* the

collinear AF order modify the quasiparticle spectrum. To investigate this problem we adopt a minimal two-band model for the quasiparticles, which can be described by the tight binding Hamiltonian

$$\hat{H}_{qp} = \sum_{\langle i,j\rangle,\alpha\beta} t_{ij}^{\alpha\beta}\ (d_{i,\sigma}^{\alpha})^{\dagger}(d_{j,\sigma}^{\beta}) + h.c., \qquad (9)$$

where $(d_{i,\sigma}^{\alpha})^{\dagger}$ creates an electron/hole at the site i, with orbital character $\alpha = d_{xz}, d_{yz}$ and spin projection σ. The values of the four hopping amplitudes, two for direct $d_{xz,yz}-d_{xz,yz}$ hopping and two for crossed $d_{xz,yz}-d_{yz-xz}$, and $d_{yz,xz}-d_{xz,yz}$, with different signs, and are the same as used in [11]. Finally, the coupling between iron itinerant carriers to the iron local moments is done via [10]

$$\hat{H}_{Hund} = -\frac{J_H}{2}\sum_{i,\alpha}(d_{i,\sigma}^{\alpha})^{\dagger}\vec{\tau}(d_{i,\sigma}^{\alpha})\cdot\hat{\mathbf{S}}_i, \qquad (10)$$

where $\vec{\tau}$ are the Pauli matrices and J_H is the ferromagnetic Hund's exchange coupling constant.

In order to calculate the quasiparticle spectrum we make use of a semiclassical approximation. We split the sum over lattice sites i in (10) into sums over sublattices i_A and i_B, and we then replace $\hat{\mathbf{S}}_{A,B}$ by their static equilibrium configuration within the colinear AF ordered state. The total quasiparticle Hamiltonian $\hat{H}_{qp} + \hat{H}_{Hund}$ is then quadratic in the $(d_{i,\sigma}^{\alpha})^{\dagger}, (d_{i,\sigma}^{\alpha})$ operators and can be easily diagonalized. The eigenvalues are plotted in Fig. 3. In the high temperature magnetically disordered phase the sublattice magnetization is zero and the dispersion is the one of the tight binding Hamiltonian $\hat{H}_{qp}$ alone, where quasiparticles are characterized by a multi-band Fermi surface, with a rather large density of states, Figs. 3a) and b). Upon collinear AF ordering, however, the doubling of the magnetic unit cell, and the consequent Brillouin zone folding, produces slightly anisotropic, hole-like Dirac cones at very specific locations, $(\pm 0.25\pi, 0)$ and $(\pm 0.75\pi, 0)$, related to the collinear structure of the AF order, see Figs. 3c) and d), thus contributing a very small density of states. These two features are consistent with both recent ARPES results, see Fig. 1 of Ref. [19], and optical spectroscopy [6], which reveal a strong reduction of the density of states upon AF ordering, for $T < T_{SDW}$ (where T_{SDW} is the spin-density-wave transition temperature). The existence of Dirac cones in iron pnictides had already been discussed in the literature [20] by using an itinerant-only model. Here, we have demonstrated that, also within a model where local moments interact with a bath of quasiparticles, such cones appear at the precise positions observed in experiments. Finally, let us remark that, from the point of view of the magnetic spectrum, the bath of carriers simply provide a width (finite magnon lifetime) to the magnetic spectral lines, without otherwise modifying the pole structure obtained in this work.

We have seen that the collinear AF ground state of the spin-Hamiltonian (1), containing two coupled, interpenetrating Néel states, gives rise to a second, optical spin-wave branch in the magnetic excitation spectrum, that can be identified as an additional step in the integrated neutron intensity in $SeFe_2As_2$ [13]. It remains to determine the specific polarization of each of the two spin-wave branches, through polarized neutron scattering, and to look for the effects of such additional optical spin-wave branch in the thermodynamic properties of the $SrFe_2As_2$ system, such as the magnetic contribution to the specific heat [12]. We have also seen that, when coupled to a bath of itinerant quasiparticles, the collinear AF order produces hole-like, slightly anisotropic Dirac cones as recently observed by ARPES in Ref. [19].

The authors acknowledge invaluable discussions with A. H. Castro Neto and Mohammed El Massalami. This work was supported by CNPq and FAPERJ.

[1] Y. Kamihara, *et al.*, J. Am. Chem. Soc. **130**, 3296 (2008).
[2] M. Rotter, M. Tegel, and D. Johrendt, Phys. Rev. Lett. **101**, 107006 (2008).
[3] M. R. Norman, Physics **1**, 21 (2008).
[4] C. Liu, *et al.*, Phys. Rev. Lett. **101**, 177005 (2008).
[5] J. Dai, Q. Si, Jian-Xin Zhu, and E. Abrahams, PNAS **106**, 4118 (2009).
[6] Peng Cheng, *et al.*, Phys. Rev. B **78**, 134508 (2008); W. Z. Hu, *et al.*, Phys. Rev. Lett. 101, 257005 (2008).
[7] F. Ma, Zhong-Yi Lu, and T. Xiang, Phys. Rev. B **78**, 224517 (2008).
[8] V. Cvetkovic and Z. Tesanovic, Eur. Phys. Lett. **85**, 37002 (2009).
[9] A. V. Chubukov, D. V. Efremov, and I. Eremin, Phys. Rev. B **78**, 134512 (2008); J. Knolle, *et al.*, preprint arXiv:1002.1668.
[10] Weicheng Lv, Frank Krüger, and Philip Phillips, preprint arXiv:1002:3165.
[11] S. Raghu, *et al.*, Phys. Rev. B **77**, 220503(R) (2008).
[12] C. M. S. da Conceição, M. B. Silva Neto, and E. C. Marino, in preparation.
[13] J. Zhao *et al.*, Phys. Rev. Lett. **101**, 167203 (2008).
[14] R. A. Ewings, *et al.*, Phys. Rev. B **78**, 220501(R) (2008).
[15] P. Chandra, P. Coleman, and A. I. Larkin, Phys. Rev. Lett. **64**, 88 (1990).
[16] C. Xu, M. Mueller, and S. Sachdev, Phys. Rev. B **78**, 020501(R) (2008).
[17] C. Fang *et al.*, Phys. Rev. B **77**, 224509 (2008).
[18] Dao-Xin Yao and E. Carlson, Phys. Rev. B **78**, 052507 (2008).
[19] P. Richard, *et al.*, Phys. Rev. Lett. **104**, 137001 (2010).
[20] Y. Ran, *et al.*, Phys. Rev. B **79**, 014505 (2009).